Journal for ImmunoTherapy of Cancer

Fibrinogen-like protein 2 promotes tumor immune suppression by regulating cholesterol metabolism in myeloid-derived suppressor cells

Lei Wu ,[1,2] Xudong Liu,[2] Juan Lei,[1] Nan Zhang,[2] Huakan Zhao,[1] Jiangang Zhang,[1] Huan Deng,[1] Yongsheng Li [1,2]

To cite: Wu L, Liu X, Lei J, *et al*. Fibrinogen-like protein 2 promotes tumor immune suppression by regulating cholesterol metabolism in myeloid-derived suppressor cells. *Journal for ImmunoTherapy of Cancer* 2023;**11**:e008081. doi:10.1136/jitc-2023-008081

► Additional supplemental material is published online only. To view, please visit the journal online (http://dx.doi.org/10.1136/jitc-2023-008081).

Accepted 20 November 2023

[1]Department of Medical Oncology, Chongqing University Cancer Hospital, Chongqing, China
[2]School of Medicine, Chongqing University, Chongqing, China

Correspondence to
Yongsheng Li; lys@cqu.edu.cn

ABSTRACT

Background Myeloid-derived suppressor cells (MDSCs) are crucial mediators of tumor-associated immune suppression. Targeting the accumulation and activation of MDSCs has been recognized as a promising approach to enhance the effectiveness of immunotherapies for different types of cancer.

Methods The MC38 and B16 tumor-bearing mouse models were established to investigate the role of Fgl2 during tumor progression. Fgl2 and FcγRIIB-deficient mice, adoptive cell transfer, RNA-sequencing and flow cytometry analysis were used to assess the role of Fgl2 on immunosuppressive activity and differentiation of MDSCs.

Results Here, we show that fibrinogen-like protein 2 (Fgl2) regulates the differentiation and immunosuppressive functions of MDSCs. The absence of Fgl2 leads to an increase in antitumor $CD8^+$ T-cell responses and a decrease in granulocytic MDSC accumulation. The regulation mechanism involves Fgl2 modulating cholesterol metabolism, which promotes the accumulation of MDSCs and immunosuppression through the production of reactive oxygen species and activation of XBP1 signaling. Inhibition of Fgl2 or cholesterol metabolism in MDSCs reduces their immunosuppressive activity and enhances differentiation. Targeting Fgl2 could potentially enhance the therapeutic efficacy of anti-PD-1 antibody in immunotherapy.

Conclusion These results suggest that Fgl2 plays a role in promoting immune suppression by modulating cholesterol metabolism and targeting Fgl2 combined with PD-1 checkpoint blockade provides a promising therapeutic strategy for antitumor therapy.

WHAT IS ALREADY KNOWN ON THIS TOPIC

⇒ Fibrinogen-like protein 2 (Fgl2) is a member of the fibrinogen family and plays immunosuppressive effects on both innate and adaptive immunity. FGL2 inhibited $CD103^+$ DC differentiation by suppressing NF-κB, STAT1/5, and p38 activation.

⇒ Although Fgl2 has been reported to play a role in promoting tumor progression in various types of cancer, the expression and function of Fgl2 in myeloid-derived suppressor cells (MDSCs) remains largely unknown.

WHAT THIS STUDY ADDS

⇒ Fgl2 regulates the activity and function of tumor-infiltrating $CD8^+$ T cells, thereby controlling anti-tumor immunity. Depleting Fgl2 can slow tumor growth by reducing the immunosuppressive activity of MDSCs.

⇒ Fgl2 promotes XBP1 signaling and cholesterol production in MDSCs, which affects their differentiation and immunosuppressive functions.

⇒ Fgl2-mediated reactive oxygen species generation promotes lipid peroxidation and constitutive XBP1 activation in MDSCs.

⇒ Combining checkpoint blockade with Fgl2 inhibition may lead to more effective antitumor effects in vivo.

HOW THIS STUDY MIGHT AFFECT RESEARCH, PRACTICE OR POLICY

⇒ Fgl2 promotes the generation and immune suppressive effects of MDSCs via cholesterol metabolism and XBP1 signaling, which suggests an immunotherapeutic target for cancer therapy.

INTRODUCTION

The tumor microenvironment (TME) is a complex environment consisting of tumor cells, immune cells, secreted factors, the extracellular matrix, and metabolic molecules.[1] Several studies have shown that TME plays a crucial role in tumorigenesis, metastasis, and response to immunotherapy and chemotherapy.[2] The TME is characterized by the infiltration of various immune suppressor cells, such as regulatory T-cells (Tregs), tumor-associated macrophages (TAMs), and myeloid-derived suppressor cells (MDSCs).[3] MDSCs are a group of heterogeneous immature myeloid cells that play a crucial role in immunosuppression within the TME.[4] Within the TME, cytokines, such as granulocyte-macrophage colony-stimulating factor (GM-CSF) and IL-6, stimulate the differentiation of MDSCs from multipotent hematopoietic progenitor cells (HPCs) by activating the STAT3 and STAT5 pathways.[5 6] Following the release of

inflammatory cytokines and factors, such as toll-like receptor ligands and prostaglandin E_2 (PGE_2), MDSCs are activated and expanded through the STAT1 and NF-κB pathways.[4 7]

MDSCs can be divided into two subgroups: granulocytic MDSCs (G-MDSCs) and monocytic MDSCs (M-MDSCs). Both subgroups can suppress immune responses in the TME through various mechanisms.[4] MDSCs express high levels of immunosuppressive molecules such as Arginase 1 (Arg-1), inducible nitric oxide synthase (iNOS), reactive oxygen species (ROS), and Programmed death ligand 1 (PD-L1), which inhibit the activation of $CD4^+$ and $CD8^+$ T cells.[8] Additionally, MDSCs secrete cytokines such as IL-10 and TGFβ, which promote the induction of other immune inhibitory populations such as TAMs and Tregs.[9] Research has shown that the accumulation and activation of MDSCs are associated with tumor progression and metastasis in various types of tumors.[10] Therefore, targeting the immunosuppressive function of MDSCs or promoting their differentiation into dendritic cells (DCs) and macrophages could offer new opportunities for enhancing the effectiveness of immunotherapy.[4]

Fibrinogen-like protein 2 (Fgl2) is a member of the fibrinogen family and has been found to have immunosuppressive effects on both innate and adaptive immunity.[11] Previous studies have shown that Fgl2 binds to its receptor Fc gamma receptor IIB (FcγRIIB), which prevents the maturation of $CD103^+$ DCs and B cell function, as well as the mediation of $CD8^+$ T cell apoptosis.[12 13] Increasing evidence suggests that Fgl2 plays a role in promoting tumor progression in various types of cancers, such as gliomas, breast cancer, lung cancer, and hepatocellular carcinoma.[11 14 15] However, the expression and function of Fgl2 in MDSCs remains largely unknown.

This study aimed to explore the role of Fgl2 in the immunosuppressive activity of MDSCs in the TME and its potential as a therapeutic target for cancer treatment.

METHODS

Human samples and databases

Peripheral blood samples were collected from healthy adult volunteers and patients with colorectal cancer (CRC) at Chongqing University Cancer Hospital in China. The experiments were conducted in compliance with local, national, and international regulations. All patients provided written informed consent in accordance with the Declaration of Helsinki before enrollment in the study. Mononuclear cells were freshly isolated from peripheral blood using lymphocyte separation medium. All available RNA-seq data of patients with CRC (n=597) were retrieved from cBioPortal (http://www.cbioportal.org).

Cell lines and treatment

Murine MC38 and B16F10 cells were purchased from the Type Culture Collection of the Chinese Academy of Sciences (Shanghai, China) in 2020. All cell lines were examined as Mycoplasma-free using the MycAwayTM-Color One-Step Mycoplasma Detection Kit (Yeasen Biotechnology), and the most recent date of testing was April 8, 2022. The cells were authenticated and certified by ChengDu Nuohe Biotech (Sichuan, China). Mouse Breast Carcinoma Cells 4T1 were from Beyotime (Cat. No. C7218, Shanghai, China). The cells were cultured in Dulbecco's modified eagle medium (DMEM) with high glucose supplemented with 10% Fetal Bovine Serum (FBS) and 100 U/mL penicillin/streptomycin. To obtain bone marrow (BM)-derived MDSCs, $Gr\text{-}1^+$ BM cells were separated from 8 to 10 week wild-type (WT) or knockout (KO) mice using BD anti-mouse Gr-1 particles (Cat. No. 558111, BD Biosciences). The harvested cells were cultured in RPMI1640 medium containing 10% FBS supplemented with 20 ng/mL GM-CSF (Cat. No. 315-03, PeproTech) and IL-6 (Cat. No. 216-16, PeproTech) for 3 days to obtain MDSCs. For BM differentiation assays, BM cells from 8 to 10 week WT mice were cultured in RPMI1640 medium containing 10% FBS supplemented with 20 ng/mL GM-CSF and IL-6 for 3 days. For some assays, BM cells were treated with crosslinked Mouse IgG, Fgl2 (20 ng/mL, Cat. No. 10691-FL, R&D Systems), cholesterol (0.75 µg/mL, Sigma-Aldrich), *tert*-Butyl hydroperoxide solution (TBH, 300 µM, Sigma), vitamin E (60 µM; Cat. No. HY-N0683, MedChemExpress) and hydralazine (100 µg/mL; Cat. No. HY-B0464A, MedChemExpress) supplemented with GM-CSF and IL-6 for 3 days.

Animals and tumor models

Six-week-old C57BL/6 (WT) and nude mice were obtained from the Animal Institute of the Academy of Medical Sciences (Beijing, China). $Fgl2^{-/-}$ (KO) mice were kindly provided by S. Smiley (The Trudeau Institute, New York, USA), $FcγRIIb^{-/-}$ mice were obtained from J.S. Verbeek (Leiden University Medical Center, The Netherlands). Six-week-old BALB/c mice were purchased from Beijing Vital River Laboratory Animal Technology (China). The mice were maintained in a controlled environment, free from specific pathogens, and subjected to a 12-hour light cycle. They were fed a regular chow diet at the Chongqing University Cancer Hospital. For animal experiments, 6–8 week-old female mice were randomly assigned to different groups, MC38, B16F10 or 4T1 cells were subcutaneously implanted into C57BL/6, BALB/c or nude mice. The tumor size was measured using calipers every 3–4 days. The tumor volume was calculated as follows: $V = (\text{length} \times \text{width}^2) \times 0.5$. For in vivo treatment with anti-CD8 antibody (200 µg, Cat. No. BE0117, BioXcell) and an anti-Fgl2 antibody (100 µg/kg, Cat. No. FGL22-A, Alpha Diagnostic International), anti-PD-L1 antibody (200 µg, Cat. No. BE0101, BioXcell), treatment was administered intraperitoneally every 3 days starting at tumors of approximately 100 mm^3 until the mice were sacrificed. The BM reconstitution assay was performed as previously described.[16] The ethics Committee of the Chongqing University Cancer Hospital in China approved all animal experiments (Chongqing, China, CZLS202107-A). These experiments were conducted in accordance with the national and international guidelines for the care and use of laboratory animals. The Animal Care and Use Committee (IACUC) of Chongqing

University Cancer Hospital approved this study, which complied with the Declaration of Helsinki.

Seahorse analyses

BM-derived MDSCs were subjected to Seahorse analyses using the Seahorse XF Cell Mito Stress Test Kit (Cat. No. 103010-100, Agilent) as previously described.[17]

Flow cytometry (FCM)

Single-cell suspension samples isolated from the tumor, spleen, and BM were collected and preincubated in PBS containing 2% FBS for at least 20 min on ice. The cells were then labeled with the indicated antibodies (1:100) for 30 min. Dead cells were excluded using a Fixable Viability Dye Efluor 780 (Cat. No. 65-0865-14; eBioscience). The panel of antibodies used in these experiments included CD8α (Cat. No. 100706), IFN-γ (Cat. No. 505810), granzyme B (GzmB; Cat. No. 515403), Tim-3 (Cat. No. 134008), CD3 (Cat. No. 100206), CD4 (Cat. No. 100412), CD11b (Cat. No. 101208), Gr-1 (Cat. No. 108426), Ly6G (Cat. No. 127626), Ly6C (Cat. No. 128008), CD11c (Cat. No. 117308), MHC II (Cat. No. 107616), F4/80 (Cat. No. 123116), CD19 (Cat. No. 115512), PD-L1 (Cat. No. 124308), CD45.1 (Cat. No. 110708), CD45.2 (Cat. No. 109814), Sca-1 (Cat. No. 108106), c-kit (Cat. No. 105808), CD16/32 (Cat. No. 101331), CD34 (Cat. No. 119310) and CD33 (Cat. No. 303414), HLA-DR (Cat. No. 307610), all from Biolegend (San Diego, California, USA). Lineage (Cat. No. 561317) and XBP1s (Cat. No. 562642) were purchased from BD Pharmingen. For intracellular staining of Fgl2 (Cat. No. H00010875-M01, Novus), Foxp3 (Cat. No. 14-5773-82, eBioscience), ARG1 (Cat. No. 42284, GeneTex) and iNOS (Cat. No. MA5-17139, Thermo), Phospho-STAT3 (Cat. No. 9145, CST) cells were stained with surface markers, fixed, and permeabilized using the Foxp3/Transcription Factor Staining Kit (Cat. No. 00-5523-00, eBioscience), followed by intracellular antibody staining. The proliferation and functional assays of $CD8^+$ T cells were performed as described previously.[16] Cells were then collected by trypsinization and washed twice with PBS followed by re-suspending in 500 µL of PBS. The 5 , 6- carboxyfluorescein diacetate , succinimidyl ester (CFSE) probe was obtained from Dojindo (Cat. No. C309). Lipid peroxidation detection was performed using C11-BODIPY$^{581/591}$ (Cat. No. D3861, Invitrogen) according to the manufacturer's protocols. Cellular cholesterol detection was performed using the Cholesterol Cell-Based Detection Assay kit (Cat. No. 10009779, Cayman). FCM was performed on BD FACS Canto II platforms, and the results were analyzed with FlowJo software V.10.0.7 (TreeStar). MDSCs separated from MC38 tumor tissues was performed using the BD FACSAria II instrument (BD Biosciences). The purity of all populations was >95%.

Lipidomics analyses

Individual lipid species from WT and Fgl2-KO MDSCs were extracted,and lipidomic analysis was performed by Applied Protein Technology Company as previously described.[18]

Transfection assays

Lentivectors containing Fgl2 shRNAs or Fgl2 overexpression fragment lentiviral were obtained from GeneChem (Shanghai, China). MC38 cells were plated in 12-well plates and transduced with lentiviral particles at multiplicity of infection (MOI) of 100 with 5 µg/mL Polybrene (GenePharma). The cells were screened by puromycin and used for further experiments. For MDSC transfection assays, three pLKD-CMV-mcherry-2A containing shRNAs targeting Xbp1, Hmgcr or LV11-CMV-MCS-hPGK-mCherry-Puro lentivectors containing Fgl2-overexpression fragment were obtained from GenePharma (Shanghai, China). $Gr1^+$ cells were sorted from mouse BM and plated at 1×10^6 cells/mL in 12-well plates. Then, the cells were transduced with lentiviral particles at MOI of 100 with 5 µg/mL Polybrene (GenePharma). Cells were cultured for 3 days after transfection, the mCherry fluorescence was observed under an inverted fluorescence microscope. Cells were harvested and used for further experiments.

Quantitative real-time PCR (qPCR)

Total RNA was extracted from the cells using RNAiso Plus (Cat. No. 9108Q, Takara), and the RNA concentration was measured using a NanoDrop 2000 (Thermo Scientific). Total RNA (1 µg of total RNA) was converted into complementary DNA (cDNA) using the PrimeScript RT-PCR Kit (Cat. No. RR014A, Takara). qPCR was performed using the TB Green Fast qPCR Mix Kit (Cat. No. RR430A, Takara). All qPCR experiments were repeated at least thrice. All primer sequences were obtained from PrimerBank (https://pga.mgh.harvard.edu/primerbank/).

RNA sequencing library construction

Total RNA was extracted from WT and *Fgl2*$^{-/-}$ MDSCs isolated from shFgl2 MC38 tumor-bearing mice. The RNA-seq library for these RNA samples was constructed according to a strand-specific RNA sequencing library preparation protocol. The mRNA transcripts were enriched by two rounds of poly-(A^+) selection with Dynabeads oligo-(dT) 25 (Invitrogen) before library construction. The prepared libraries were sequenced on an Illumina NovaSeq 6000 platform.

Western blotting

Cells were lysed using RIPA lysis buffer, and the lysates were incubated on ice for 30 min and centrifuged at 13,000×g at 4°C for 15 min before the supernatant was collected. Western blot analysis was performed as previously described.[16] The primary antibodies included Fgl2 (1:1000; Cat. No. H00010875-M01, Novus) and β-actin (1:1000; Cat. No. A1978, Sigma-Aldrich).

Statistical analysis

Statistical methods and n values are indicated in the figure legends. All results were confirmed in at least

three independent experiments and are expressed as the mean±SD. For comparison of two groups, unpaired two-tailed Student's t-test or one-way or two-way analysis of variance (ANOVA) with Sidak multiple comparisons test were used to calculate statistical significance using GraphPad Prism software (V.8.0). For survival analysis, the Kaplan-Meier method was used, and differences in survival curves were analyzed using the log-rank test. P value <0.05 was considered statistically significant.

Data availability

The full RNA-seq dataset was uploaded to the NCBI Sequence Read Archive (SRA) database (accession code: PRJNA980623).

RESULTS

Fgl2 controls CD8⁺ T cell-dependent antitumor growth in immunocompetent mice

To investigate the role of Fgl2 in tumor growth, we generated Fgl2 knockdown (shFgl2) MC38 tumor cells and inoculated them into C57BL/6 mice. The results showed that Fgl2 knockdown tumor cells exhibited significantly slower tumor growth and prolonged survival than control tumors (figure 1A and online supplemental figure S1A,B). However, Fgl2 knockdown failed to limit MC38 tumor growth in immunodeficient nude mice (figure 1B). In contrast, Fgl2 overexpression or Fgl2 treatment significantly promoted tumor growth in C57BL/6 mice (figure 1C and online supplemental figure figure S1C,D). Notably, no significant differences in cell proliferation or cell cycle were observed between shCtrl and shFgl2 MC38 cells (online supplemental figure S1E,F). These results support our hypothesis that Fgl2 alters the immune response in the TME rather than affecting the tumor cell itself.

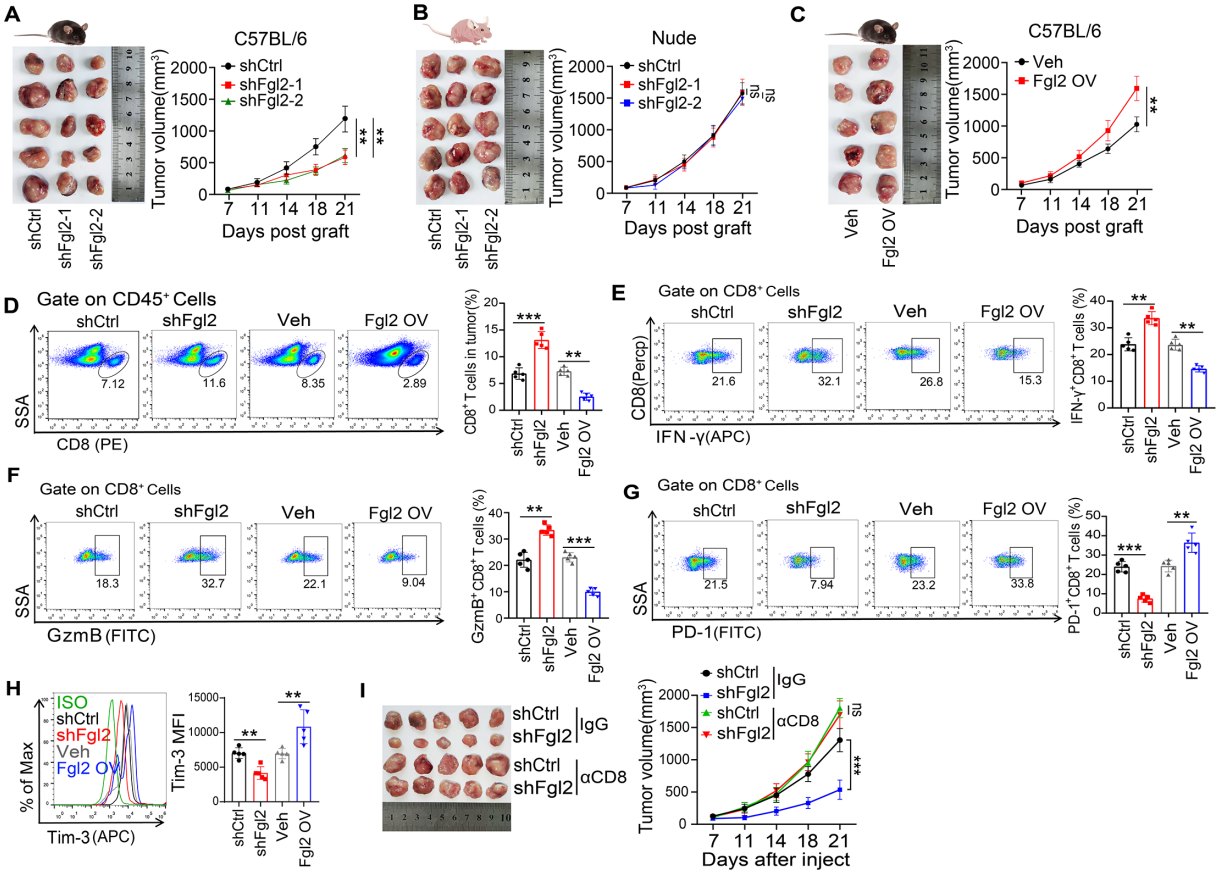

Figure 1 Fgl2 facilitates tumor growth by suppressing the infiltration of CD8⁺ T cells in the TME. (A, B) A total of 1×10⁶ shCtrl or shFgl2 transduced MC38 tumor cells were subcutaneously injected into C57BL/6 mice (A) or nude mice (B), and tumor growth was monitored every three or 4 days (n=5). (C) C57BL/6 mice were injected subcutaneously with empty vehicle (Veh) or Fgl2 overexpressed (Fgl2 OV) MC38 tumor cells and tumor volumes were measured. (D–H) C57BL/6 mice were injected subcutaneously with sh-Ctrl, sh-Fgl2, Veh, or Fgl2 OV MC38 tumor cells, and representative flow staining of CD8⁺ T cells (D), IFNγ⁺ (E), GzmB⁺ (F), PD-1⁺ (G) and Tim-3⁺ (H) CD8⁺ T cells in tumor xenografts of the indicated groups (n=5). (I) C57BL/6 mice were injected subcutaneously with shCtrl or shFgl2 MC38 tumor cells with IgG or CD8 depleting antibodies, tumor volumes were measured (n=5). **p<0.01; ***p<0.001; ns, no significant difference. Two-tailed unpaired Student's t-test (B–H) and one-way analysis of variance with Tukey multiple comparison (A, I) were performed. Fgl2, fibrinogen-like protein 2; TME, tumor microenvironment.

Next, we analyzed the effect of Fgl2 on tumor growth with respect to T cells. The percentage of tumor-infiltrating $CD8^+$ T cells in the TME was examined, and we found that Fgl2 knockdown increased $CD8^+$ T cell infiltration, whereas Fgl2 overexpression limited it (figure 1D). Additionally, Fgl2 knockdown led to an increase in IFNγ-producing and GzmB-producing $CD8^+$ T cells and a decrease in exhausted PD-1^+ and Tim-3^+ T cells (figure 1E–H). In contrast, Fgl2 overexpression in MC38 tumor cells inhibits $CD8^+$ T cell activation and function (figure 1E and F). Strikingly, we found that the antitumor response mediated by Fgl2 knockdown was completely eliminated by the depletion of $CD8^+$ T cells (figure 1I), indicating that Fgl2 regulates the activity and function of tumor-infiltrating $CD8^+$ T cells, thereby controlling antitumor immunity.

Deficiency of Fgl2 impairs MDSC infiltration and tumorigenesis

In the TME, Fgl2 is expressed by tumor cells and various immune cells, including macrophages, DCs, and Tregs.[19] To investigate the role of Fgl2 in $CD8^+$ T cell-dependent tumor control, we injected shFgl2 MC38 tumor cells subcutaneously into both WT and *Fgl2*$^{-/-}$ mice. We observed a similar level of tumor inhibition in *Fgl2*$^{-/-}$ mice compared with that in WT mice (figure 2A). Tumors from *Fgl2*$^{-/-}$ mice exhibited higher levels of immune infiltrates, specifically $CD8^+$ cytotoxic T cells (figure 2B and C), indicating an enhanced immunosurveillance response in the absence of Fgl2. Fgl2 deficiency reduced the frequencies of $CD11b^+Gr\text{-}1^+$ MDSCs in MC38 tumor-bearing mice (figure 2D). Further analysis revealed that the subset of G-MDSCs was significantly decreased in KO mice, while the proportion of M-MDSC subpopulation remained less changed. This indicates that the decreased proportion of MDSCs in KO mice was primarily due to a decrease in G-MDSCs (figure 2E and F and supplemental figure S2A). Accordingly, there was increased infiltration of DCs and M1 polarized TAMs in tumors from *Fgl2*$^{-/-}$ mice (online supplemental figure S2A-E). Next, we sought to investigate the impact of Fgl2 deficiency in tumor cells on the TME of transplanted tumors. Consistent with our expectations, we found that the absence of Fgl2 in MC38 tumor cells resulted in a reduction of tumor-infiltrating G-MDSCs and enhanced antitumor immune response (online supplemental figure S2F,G). Similarly, the percentage of G-MDSCs in B16F10 tumors from *Fgl2*$^{-/-}$ mice was significantly lower than that in WT tumors (online supplemental figure S2H,I). MDSCs play a major immunosuppressive roles in antitumor immune responses and can differentiate into macrophages and DCs.[20] The decrease in tumor-infiltrating MDSCs observed in Fgl2-deficient mice suggests that alterations in MDSCs may contribute to the retardation of tumor growth. Interestingly, there were no significant changes in iNOS and Arg-1 levels in G-MDSCs from WT and KO mice (figure 2G and online supplemental figure S2J). However, MDSCs from *Fgl2*$^{-/-}$ tumor-bearing mice showed decreased activation and expansion markers, including PD-L1, Stat3 and ROS (figure 2H–J). In addition, when Fgl2-KO G-MDSCs were co-cultivated, there was a significant increase in the proportion of IFNγ and GzmB producing $CD8^+$ T cells compared with co-cultivation with WT G-MDSCs (figure 2K and L). Fgl2-KO G-MDSCs demonstrated less effectiveness in suppressing anti-CD3 and anti-CD28-induced CD8+T cell proliferation compared with G-MDSCs with normal Fgl2 (figure 2M). These results indicate that depleting Fgl2 can slow tumor growth by reducing the accumulation and immunosuppressive activity of MDSCs.

Fgl2 promotes MDSC differentiation from HPCs in the TME

We next investigated whether Fgl2 plays a role in MDSC chemotaxis by examining the difference in chemotaxis-related genes between WT and Fgl2-deficient mice. The results showed no significant difference in the expression levels of these genes, indicating that decreased MDSCs in tumors may not be due to increased cell chemotaxis (online supplemental figure S3A). However, Fgl2 deficiency resulted in a systemic decrease in $CD11b^+$ $Gr1^+$ populations and $CD11b^+$ $Ly6G^+$ subset in the BM, peripheral blood, and spleen as the tumor progressed (figure 3A–D and online supplemental figure S3B,C). Consistent with these findings, the absence of Fgl2 in BM cells led to a reduction in the proportion of granulocyte/macrophage progenitors (GMPs) in the population of HPCs (figure 3E), which are responsible for the expansion of MDSCs.[2 21 22] To test the hypothesis that Fgl2 may promote the differentiation of MDSCs from HPCs, BM cells were cultured with Fgl2 supplementation for MDSC induction, and the differentiation of MDSCs was measured. The results showed an increase in the proportion of G-MDSCs after Fgl2 treatment (figure 3F and online supplemental figure S3D). Conversely, Fgl2-deficient BM cells yielded reduced numbers of G-MDSCs and an increase in the presence of macrophages and DCs than WT BM, suggesting that Fgl2 may be responsible for the generation of G-MDSCs (figure 3G and online supplemental figure S3E). Previous studies have shown that FcγRIIB is a receptor of Fgl2,[13] to determine whether Fgl2-mediated MDSC differentiation was dependent on FcγRIIB, WT and FcγRIIB$^{-/-}$ BM cells were stimulated with Fgl2 during MDSC induction. The addition of Fgl2 increased the proportion of G-MDSCs among WT BM cells, but not among FcγRIIB$^{-/-}$ BM cells (figure 3H–J). Importantly, the administration of cross-linked IgG did not have any effect on the expansion of MDSC populations (online supplemental figure S3F). This suggests that Fgl2 is involved in the differentiation of HPCs in a manner that depends on FcγRIIB.

To assess the impact of Fgl2 on MDSC differentiation in vivo, we conducted a co-adoptive transfer of both WT and *Fgl2*$^{-/-}$ BM cells into congenic hosts (online supplemental figure S3G). The frequencies of MDSCs, macrophages, and DCs in the tumor were measured on day 21 post-transplantation. We observed that tumor growth was inhibited in KO→KO BM chimeric mice compared

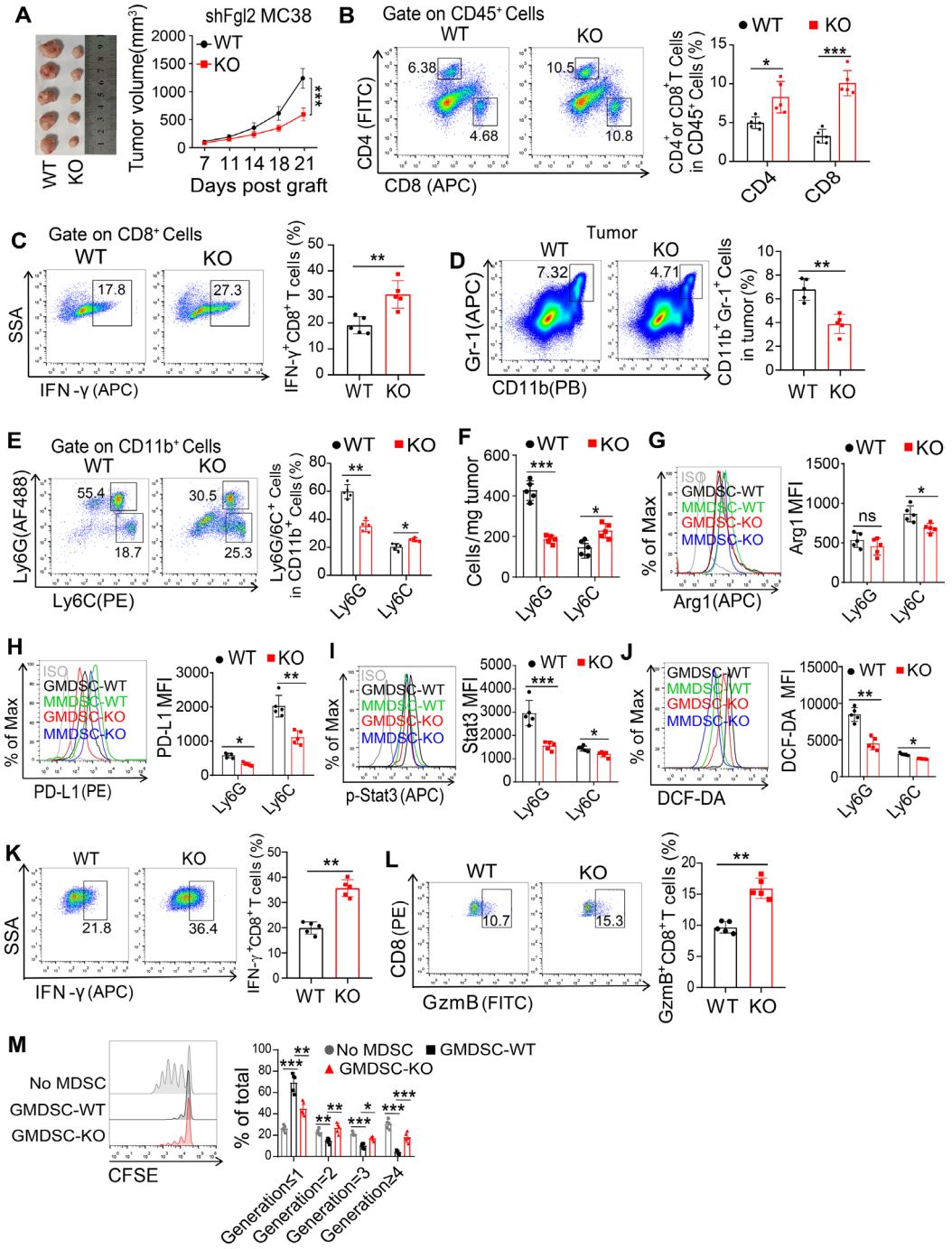

Figure 2 Fgl2 deficiency inhibited the expansion and immunosuppressive activity of MDSCs. (A) C57BL/6 (WT) or Fgl2$^{-/-}$ (KO) mice were subcutaneously injected with 10^6 shFgl2 MC38 tumor cells. Tumor growth was monitored at indicated time points (n=5). (B, C) WT or KO mice were sacrificed on day 14 post-xenograft of shFgl2 MC38 cells, and the frequency of CD4$^+$ and CD8$^+$ T cells (B) and IFN-γ-producing CD8$^+$ T cells (C) in tumors was analyzed by FCM. Data are representative of three independent experiments, n=5. (D–F) The frequency of CD11b$^+$Gr1$^+$ MDSCs (D), G-MDSC and M-MDSC subpopulations (E), absolute number of MDSCs (F) from WT and KO shFgl2 MC38 tumor tissues were determined. (G–J) Arg1 (G), PD-L1 (H), p-Stat3 (Tyr705) (I) and DCF-DA (J) expression in G-MDSCs and M-MDSCs from WT and KO shFgl2 MC38 tumor tissues were determined using FCM (n = 5). (K, L) CD8$^+$ T lymphocytes were obtained from the spleen of naïve mice and were then co-cultured with WT/ KO MDSCs that were sorted from shFgl2 MC38 tumor tissues, in a ratio of 2:1. After 48 hours, the frequencies of IFN-γ$^+$ (K) and GzmB$^+$ (L) T cells were determined using FCM (n=5). (M) CD8$^+$ T-cell proliferation suppression assay. CFSE-labeled CD8$^+$ T lymphocytes from the spleen of naive mice were stimulated with anti-CD3 and anti-CD28 antibodies. These cells were then co-cultured with G-MDSCs sorted from shFgl2 MC38 tumor tissues of WT and KO mice, at a ratio of 2:1, for a duration of 3 days. Anti-CD3 and anti-CD28 induced proliferation of CD8$^+$ T cells were measured by FCM; n=5. Data are expressed as mean±SD. *p<0.05, **p<0.01, ***p<0.001 ns, no significant difference, by two-tailed unpaired Student's t-test. Fgl2, fibrinogen-like protein 2; FCM, flow cytometry; KO, knockout; G-MDSCs, granulocytic myeloid-derived suppressor cells; MDSCs, myeloid-derived suppressor cells; M-MDSCs, monocytic myeloid-derived suppressor cells; WT, wild-type.

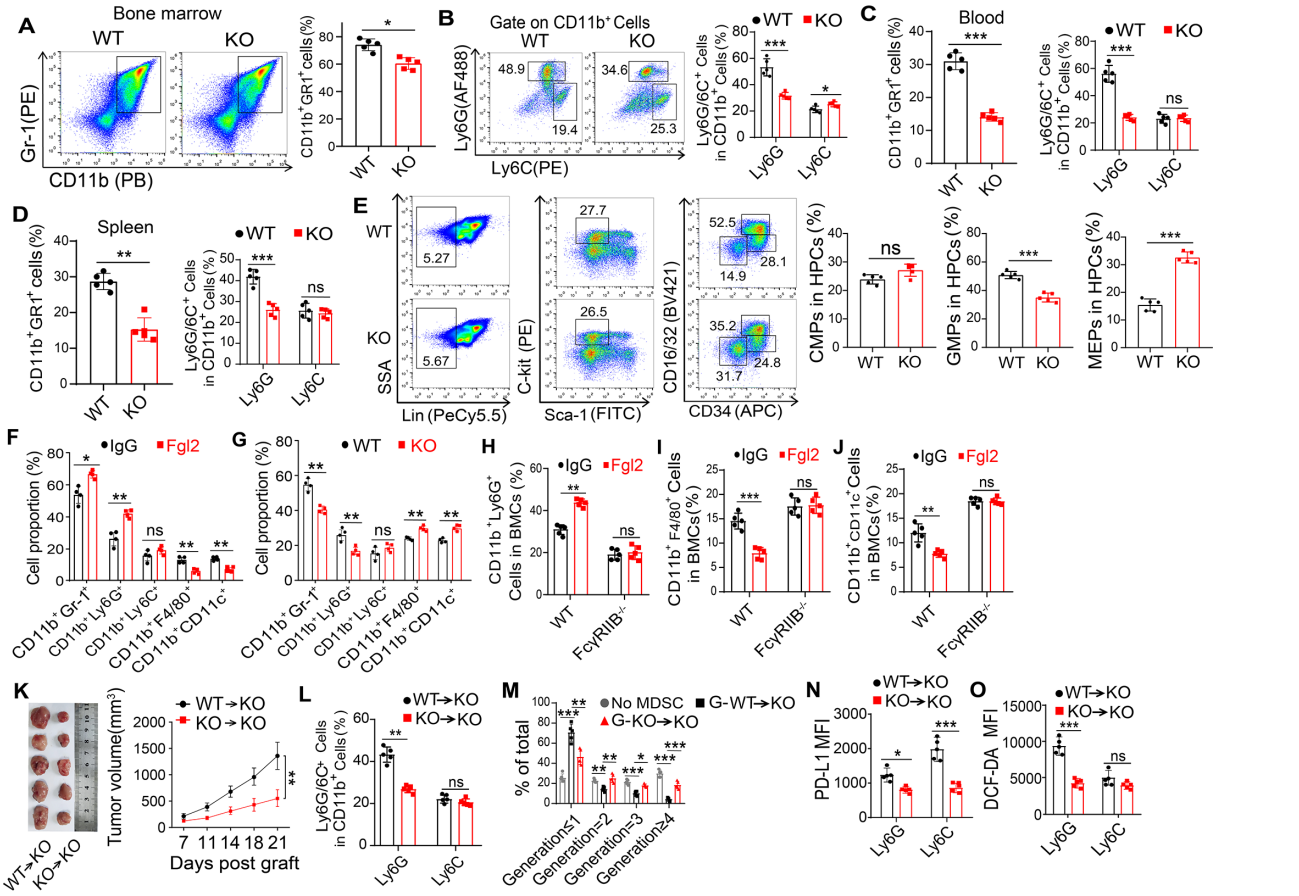

Figure 3 Fgl2 contributes to MDSC generation in the tumor-bearing mice. (A–D) The percentages of $CD11b^+Gr1^+$, $CD11b^+Ly6G^+$, and $CD11b^+Ly6C^+$ cells in BM (A, B), peripheral blood (C), and spleen (D) from WT and KO shFgl2 MC38 tumor-bearing mice were detected, n=5. (E) The percentages of GMP ($Lin^-Sca\text{-}1^-C\text{-}kit^+CD16/32^+CD34^+$), common myeloid progenitor (CMP; $Lin^-Sca\text{-}1^-C\text{-}kit^+CD16/32^{int}CD34^+$), and megakaryocyte/erythrocyte progenitor (MEP; $Lin^-Sca\text{-}1^-C\text{-}kit^-CD16/32^-CD34^-$) subpopulations in HPCs from WT and KO tumor-bearing mice, n=5. (F) WT BMs were treated with GM-CSF (20 ng/mL) and IL-6 (20 ng/mL) in the presence of IgG or Fgl2 (20 ng/mL), and the ratio of MDSCs, DCs, and macrophages was analyzed after 3 days (n=4). (G) WT and KO BMs were treated with GM-CSF (20 ng/mL) and IL-6 (20 ng/mL) for 3 days, and the MDSCs, DCs, and macrophage ratios were assessed (n=4). (H–J) WT and FcγRIIb KO BMs were treated with GM-CSF/IL-6 (20 ng/mL) to induce MDSC differentiation for 3 days in the presence IgG (1.0 µg/mL) or Fgl2 (20 ng/mL). Then, cells were harvested, MDSCs (H), macrophages (I) and DCs (J) were assessed, n=5. (K, L) *Fgl2*$^{-/-}$ recipient mice were irradiated and received WT or *Fgl2*$^{-/-}$ BM cells for the BM reconstitution experiment. Two weeks after BM chimera reconstitution, the mice were injected subcutaneously with 10^6 shFgl2 MC38 cells. Tumor growth was monitored at indicated time points (K). The frequency of tumor-infiltrating G-MDSCs and M-MDSCs (L) were assessed (n=5). (M–O) CFSE-labeled $CD8^+$ T cells were co-cultured with G-MDSCs sorted from tumors of BM chimeric mice for 3 days. The proliferation of $CD8^+$ T cells was measured by FCM; (M, n=5). PD-L1 expression (N) and ROS (O) levels in G-MDSCs and M-MDSCs in tumors from BM chimeric mice were assessed (n=5). Data are expressed as mean±SD. *p<0.05; **p<0.01; ***p<0.001; ns, no significant difference, by two-tailed unpaired Student's t-test. BM, bone marrow; DCs, dendritic cells; FCM, flow cytometry; Fgl2, fibrinogen-like protein 2; G-MDSCs, granulocytic myeloid-derived suppressor cells; KO, knockout; M-MDSCs, monocytic myeloid-derived suppressor cells; ROS, reactive oxygen species; WT, wild-type.

with WT→KO BM chimeric mice (figure 3K). There was a noticeable decrease in the number of G-MDSCs, but there was a significant increase in the presence of $CD8^+$ T lymphocytes, macrophages, and DCs in the *Fgl2*$^{-/-}$ BM transferred mice (figure 3K and L and online supplemental figure S3H-K). This suggests that Fgl2-deficient BM cells have a reduced ability to differentiate into G-MDSCs. Furthermore, we found that G-MDSCs collected from tumor tissue of WT→KO BM chimeric mice were more effective in suppressing $CD8^+$ T cell proliferation (figure 3M). These MDSCs expressed significantly higher levels of Fgl2, PD-L1, and ROS compared with those from KO→KO BM chimeric mice in the TME (figure 3N and O and online supplemental figure S3H). Therefore, these findings indicate that Fgl2 promotes GMP differentiation towards the granulocytic lineage, leading to the development of G-MDSCs.[23]

Fgl2 promotes HPC differentiation into MDSCs via cholesterol metabolism

Tumor-infiltrating MDSCs undergo metabolic reprogramming to adapt the oxygen-limited and nutrient-limited

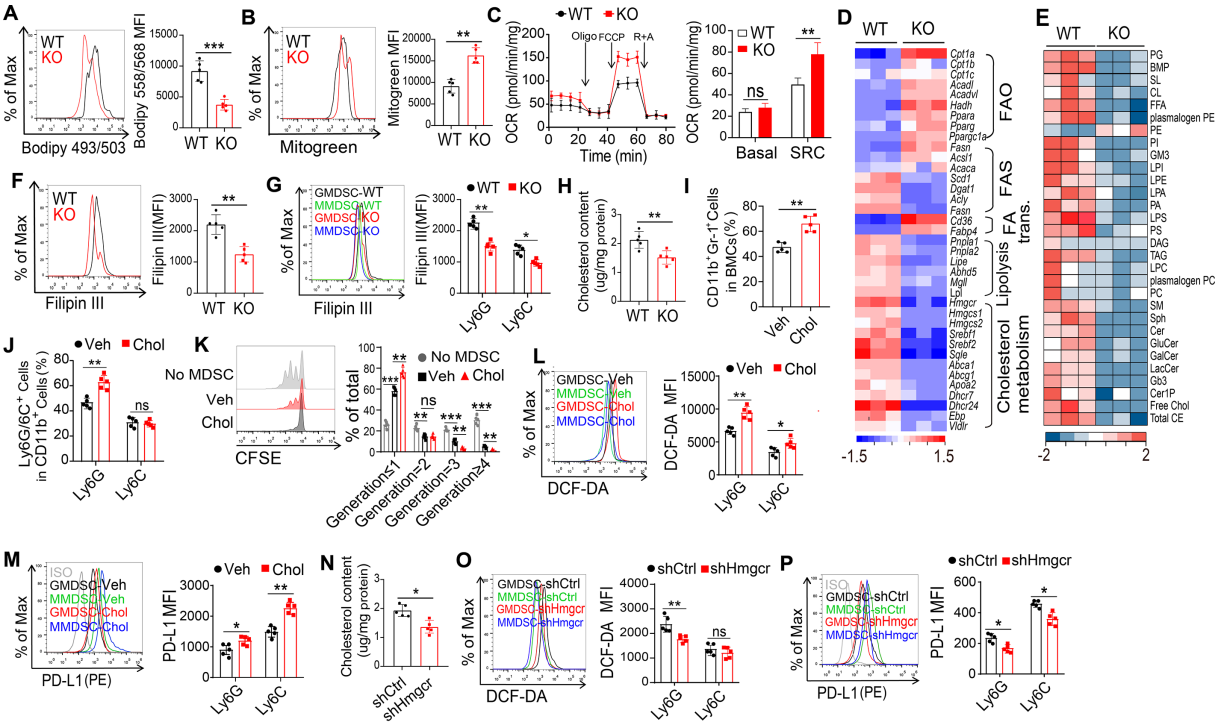

Figure 4 Fgl2 promotes differentiation and immunosuppression function of MDSCs via cholesterol metabolism. (A) Bodipy 493/503 staining of WT and Fgl2-KO MDSCs from shFgl2 MC38 tumors; n=5. (B) MitoGreen staining of WT and Fgl2-KO MDSCs. (C) Oxygen consumption rate (OCR) and spare respiratory capacity (SRC) of WT and Fgl2-KO MDSCs were measured using a Seahorse XFe 96 analyzer (n=3). (D) The expression of key genes involved in FAO, fatty acid synthesis (FAS), fatty acid transport, lipolysis, and cholesterol metabolism is displayed in a heat map. (E) Lipidomic analysis of WT and Fgl2-KO MDSCs. (F–H) Filipin III staining of MDSCs (F), Filipin III staining of G-MDSCs and M-MDSCs in CD11b$^+$ cells (G) and cholesterol content of MDSCs (H) from WT and Fgl2-KO shFgl2 MC38 tumors, n=5. (I, J) BM cells isolated from the femurs of WT mouse were cultured in RPMI1640 medium with 20 ng/mL GM-CSF and 20 ng/mL IL-6 for 3 days. Then, cells were treated with 0.75 mg/mL cholesterol for 48 hours, the percentage of MDSCs (I), G-MDSCs and M-MDSCs in CD11b$^+$ cells (J) were determined by FCM. (K) G-MDSCs sorted from spleen of MC38 tumor-bearing mice were cultured in RPMI1640 medium with vehicle (Veh, 0.1% ethanol) or 0.75 µg/mL cholesterol for 48 hours. MDSCs were then co-cultured with CD8$^+$ T cells, Anti-CD3 and anti-CD28 induced proliferation of CD8$^+$ T cells were measured by FCM; n=5. (L, M) MDSCs isolated from spleen of MC38 tumor-bearing mice were cultured in medium with 0.75 µg/mL cholesterol for 24 hours, ROS (L) and PD-L1 (M) expression levels in G-MDSCs and M-MDSCs were assessed. (N–P) Gr-1$^+$ cells from the WT mice BM were transfected with control virus (sh-Ctrl) or virus expressing shRNA against Hmgcr (sh-Hmgcr), in the presence of 20 nM GM-CSF for 3 days, the cholesterol content of MDSCs (N), ROS (O) and PD-L1 (P) expression in G-MDSCs and M-MDSCs were analyzed using FCM; n=5. Data are expressed as mean±SD. *p<0.05; **p<0.01; ***p<0.001; ns, no significant difference, by two-tailed unpaired Student's t-test. FAO, fatty acid oxidation; Fgl2, fibrinogen-like protein 2; G-MDSCs, granulocytic myeloid-derived suppressor cells; KO, knockout; M-MDSCs, monocytic myeloid-derived suppressor cells; ROS, reactive oxygen species; WT, wild-type.

TME.[24] Recent studies have shown that lipid metabolism is altered in MDSCs, which plays a crucial role in their differentiation and suppressive and protumorigenic functions.[25] Therefore, we postulated that the differentiation and immunosuppressive capabilities of MDSCs mediated by Fgl2 are reliant on lipid metabolism. Indeed, we observed a decrease in intracellular lipid droplets in Fgl2-deficient tumors infiltrating MDSCs (figure 4A). Additionally, FCM analysis revealed a significant increase in the number of mitochondria in *Fgl2*$^{-/-}$ MDSCs, particularly in the m-MDSC subset (figure 4B and online supplemental figure S4A,B). Consistently, *Fgl2*$^{-/-}$ MDSCs had a higher mitochondrial oxygen consumption rate (OCR) and spare respiratory capacity (SRC) than WT MDSCs, indicating an increase in fatty acid oxidation (FAO) (figure 4C). Subsequently, we conducted qPCR analysis to examine the expression of genes related to lipid metabolism in both WT and *Fgl2*$^{-/-}$ MDSCs. The results revealed that the expression of genes related to fatty acid oxidation (*Cpt1a*, *Hadh*) and fatty acid transport (*Cd36* and *Fabp4*) was increased, whereas genes associated with fatty acid synthesis (*Fasn*, *Acsl1*, *Acaca*, *Scd1*, *Dgat1*) and lipolysis (*Lpl*, *Lipe*, *Abhd5*) were decreased. Interestingly, the mRNA levels of genes involved in cholesterol biosynthesis, including 3-hydroxy-3-methylglutaryl-CoA synthase 1 (*Hmgcs1*), HMG-CoA reductase (*Hmgcr*), and *Srebf-1/2*, were significantly reduced (figure 4D).

In line with the above results, cholesterol level and total cholesterol content were reduced in tumor-infiltrated MDSCs from *Fgl2*$^{-/-}$ mice (figure 4E–H). Lipidomic analysis also confirmed that Fgl2-deficient MDSCs showed decreased cholesterol and cholesterol ester content

(figure 4E). We next investigated whether altered cholesterol metabolism was responsible for Fgl2 mediated the differentiation and immunosuppression of MDSCs. The results showed MDSCs had higher levels of cholesterol than HPCs (online supplemental figure S4C,D). In addition, administration of cholesterol promoted BM cell differentiation into G-MDSCs, while decreasing their differentiation into mature cells (online supplemental figure S4E-H). A co-culture assay revealed that G-MDSCs treated with cholesterol exhibited enhanced suppressive function compared with MDSCs treated with the control (figure 4K). This finding was supported by an increase in the levels of signature MDSC molecules, PD-L1 and ROS, following cholesterol treatment (figure 4L and M). Subsequently, we explored the functional role of HMGCR, a cholesterol biosynthesis rate-limiting enzyme, in MDSC activation (online supplemental figure S4I). As anticipated, knockdown of *Hmgcr* resulted in a reduction in cholesterol levels as well as the expression of PD-L1 and ROS in MDSCs (figure 4N–P). These findings suggest that Fgl2-mediated differentiation and immunosuppression of MDSCs is attributed to increased cholesterol metabolism.

Fgl2 promotes cholesterol biosynthesis through XBP1 signaling

To address the molecular mechanisms underlying the effect of Fgl2 on cholesterol metabolism in tumor-infiltrating MDSCs, we conducted RNA-seq analysis. Our results revealed that Fgl2$^{-/-}$ MDSCs exhibited differential expression of 806 downregulated and 818 upregulated genes compared with WT MDSCs (figure 5A). These genes were enriched in cell leukocyte differentiation and activation pathways, which supports the notion that Fgl2 plays a vital role in regulating the differentiation and immunosuppressive functions of MDSCs (figure 5B and online supplemental figure S5A,B). Interestingly, the molecular function analysis revealed that these differentially expressed genes were closely associated with unfolded protein binding (online supplemental figure S5C). As the endoplasmic reticulum (ER) is inherently linked to protein folding and lipid biosynthesis,[26] we hypothesized that Fgl2 could potentially induce ER stress in tumor-infiltrating MDSCs.

As expected, we found that Fgl2-deficient MDSCs showed downregulation of the unfolded protein response (UPR) or ER stress signal member Xbp1 (figure 5C–E). In addition, the expression of Xbp1s was increased in tumor-infiltrating MDSCs compared with splenic-MDSCs or Gr1^{+} BM cells, accompanied by increased Fgl2 and cholesterol synthesis-related gene expression (figure 5F; online supplemental figure S5D,E). Moreover, FcγRIIB$^{-/-}$ MDSCs also exhibited decreased expression of Xbp1s and cholesterol synthesis-related genes (figure 5G), indicating that sustained Xbp1 activation in tumor-infiltrating MDSCs probably partly due to Fgl2-FcγRIIB signaling. To determine the impact of Xbp1 activation on cholesterol metabolism in MDSCs, we examined whether Xbp1 knockdown impacted cholesterol biosynthesis and MDSC differentiation. The findings showed that XBP1 knockdown resulted in fewer immature G-MDSCs but more mature macrophages and DCs than the control group (figure 5H). We also found that Xbp1 knockdown showed a reduction of cholesterol content compared with that from shCtrl MDSCs (figure 5I). Accordingly, we also observed reduced expression of ROS and PD-L1 in Xbp1-knockdown MDSCs (figure 5J and K). These results suggested that Fgl2 promotes Xbp1 signaling and cholesterol production in MDSCs, which affects their differentiation and immunosuppressive functions.

Fgl2 promotes lipid peroxidation to activate XBP1 in MDSCs

Previous studies have demonstrated that the abnormal buildup of peroxidized lipids within cells plays a crucial role in the activation of XBP1.[27 28] Therefore, we investigated whether Fgl2 in MDSCs contributes to lipid peroxidation, leading to Xbp1 activation. To test this, we examined the levels of lipid peroxidation in MDSCs with and without Fgl2. Our results showed that MC38 tumor-infiltrating MDSCs lacking Fgl2 had lower levels of intracellular peroxidation lipids compared with MDSCs with Fgl2 (figure 6A). Furthermore, tumor-infiltrating MDSCs had significantly higher levels of intracellular peroxidation lipids compared with MDSCs isolated from the spleen of the same host or naïve Gr^{+} cells from the BM (figure 6B). On the other hand, overexpression of Fgl2 in MDSCs increased levels of lipid peroxidation and promoted Xbp1 activation (figure 6C and D and online supplemental figure S6A).

Excessive ROS production has been extensively documented to be responsible for intracellular lipid oxidation.[28] In line with this, MDSCs lacking Fgl2 demonstrated a decrease in ROS production (figure 2J). The expression of signature genes involved in ROS production, such as myeloperoxidase and NADPH oxidase 2 (NOX-2), were also found to be decreased in Fgl2-deficient cells (figure 6E and F). Additionally, we observed a significant increase in antioxidant enzyme glutathione peroxidase 4 (GPX4), catalase and Sod1 transcripts in Fgl2-deficient MDSCs (figure 6F and online supplemental figure S6B). Furthermore, both Fgl2 overexpression and treatment with the ROS generator TBH resulted in enhanced ROS generation, lipid peroxidation, and Xbp1 activation in MDSCs (figure 6G–I and online supplemental figure S6C). Subsequently, we explored the impact of ROS-scavenging agents on Xbp1 activation in MDSCs. Treatment with the antioxidant vitamin E or the lipid peroxidation scavenging agent hydralazine markedly decreased Xbp1 expression in MDSCs (figure 6J–L). These findings suggest that Fgl2-mediated ROS generation promotes lipid peroxidation and constitutive Xbp1 activation in MDSCs.

Inhibition of the Fgl2 enhances antitumor immune responses

To determine whether Fgl2 promotes ER stress and MDSC generation in vivo, we administered an anti-Fgl2 neutralizing antibody to tumor-bearing mice (figure 7A).

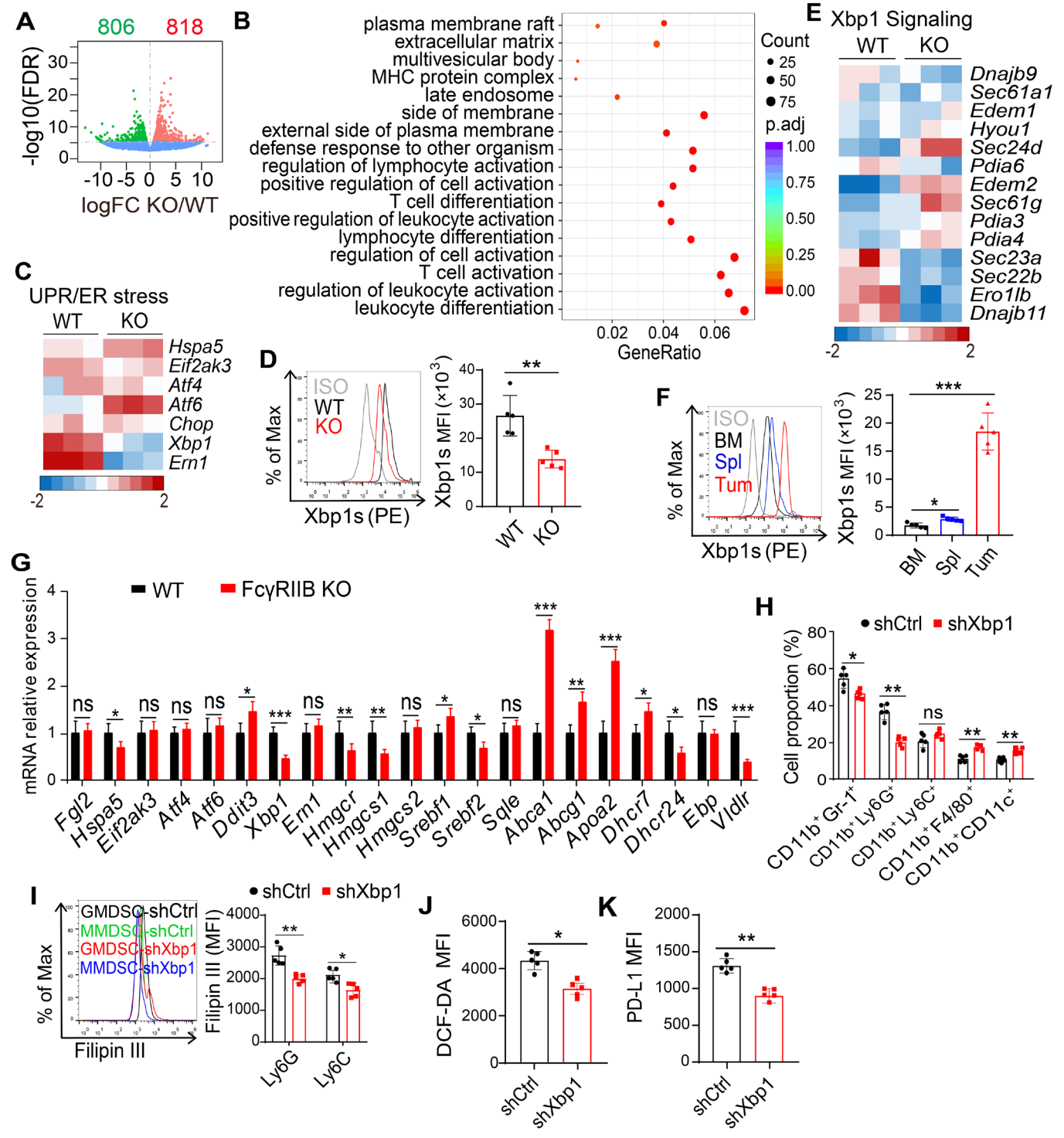

Figure 5 Fgl2 induces cholesterol production in MDSCs via XBP1 signaling. (A, B) Volcano plots (A) and GO analysis (B) of differentially expressed genes in MDSCs from WT or Fgl2 KO mice 14 days post-grafting of shFgl2 MC38 tumor cells (adjusted p≤0.01 and fold change (FC) ≥2), n=3. (C) Heatmap of differentially expressed genes involved in the UPR/ER stress pathway (n=3). (D) Intracellular Xbp1s expression in MDSCs from WT or Fgl2 KO tumor-bearing mice. (E) Heatmap of differentially expressed genes in Xbp1 signaling in WT or Fgl2 KO MDSCs, n=3. (F) Xbp1s expression in $CD11b^{+}Gr\text{-}1^{+}$ cells from the BM, spleen (Spl), and tumor (Tum) of MC38 tumor-bearing mice was analyzed. G) $CD11b^{+}Gr\text{-}1^{+}$ cells from WT and FcγRIIB KO MC38 tumor tissues were sorted, ER stress and cholesterol metabolism related genes expression were measured (n=3). (H) $Gr\text{-}1^{+}$ cells from the BM were transfected with sh-Ctrl or sh-Xbp1 lentiviral for 3 days, and the MDSCs, G-MDSCs, M-MDSCs, macrophage, and DC ratios in BM cells were analyzed using FCM; n=5. (I) Filipin III staining of sh-Ctrl or sh-Xbp1 MDSCs, n=5. (J, K) DCF-DA staining (J) and PD-L1 (K) expression in sh-Ctrl or sh-Xbp1G-MDSCs were analyzed; n=5. Data are expressed as mean±SD. *p<0.05; **p<0.01; ***p<0.001; ns, no significant difference, by two-tailed unpaired Student's t-test. BM, bone marrow; DC, dendritic cell; Fgl2, fibrinogen-like protein 2; G-MDSCs, granulocytic myeloid-derived suppressor cells; KO, knockout; M-MDSCs, monocytic myeloid-derived suppressor cells; WT, wild-type.

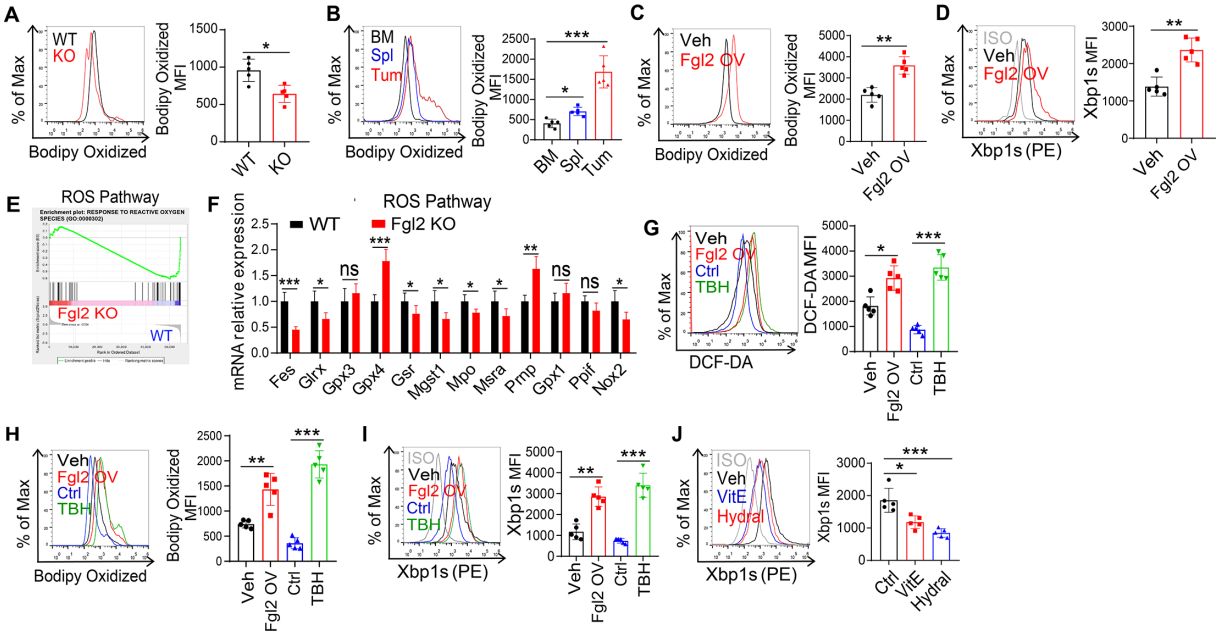

Figure 6 Fgl2 promotes ROS production, lipid peroxidation and XBP1 activation in MDSCs. (A) Lipid peroxidation levels in MDSCs from WT or Fgl2 KO mice post-grafting the shFgl2 MC38 tumor cells 14 days, n=5. (B) Lipid peroxidation levels in CD11b$^+$Gr-1$^+$ cells from naïve mice BM, Spl and MC38 tumor were analyzed by FCM, n=5. (C, D) Gr-1$^+$ cells were sorted from naïve mice BM and transfected with control or Fgl2-overexpression lentiviral for 3 days, lipid peroxidation levels (C) and Xbp1s expression (D) in CD11b$^+$Gr-1$^+$ cells were measured (n=5). (E) Enrichment plot of the ROS pathway for the comparison between Fgl2 KO and WT MDSCs from shFgl2 MC38 tumor-bearing mice. (F) The mRNA expression of genes involved in the ROS pathway in WT and Fgl2 KO MDSCs from MC38 tumor were quantified by RT-qPCR (n=3). (G–I) Gr-1$^+$ cells from mice BM were transfected with Fgl2-overexpression lentiviral for 3 days, BM-derived MDSCs were treated with TBH (300 µM) for 24 hours, ROS production (G), lipid peroxidation levels (H) and Xbp1s expression (I) in CD11b$^+$Gr-1$^+$ cells were measured. (J) BM-derived MDSCs were treated with vitamin E (VitE; 60 µM) and hydralazine (Hydral; 100 µg/mL) for 24 hours, Xbp1s expression in CD11b$^+$Gr-1$^+$ cells were determined. Data are expressed as mean±SD. *p<0.05; **p<0.01, ***p<0.001; ns, no significant difference, by two-tailed unpaired Student's t-test. BM, bone marrow; Fgl2, Fibrinogen-like protein 2; KO, knockout; MDSCs, myeloid-derived suppressor cells; ROS, reactive oxygen species.

Our results showed that the administration of Fgl2 neutralizing antibody suppressed MC38 tumor growth and prolonged survival compared with control mice (figure 7B). Moreover, Fgl2 neutralizing antibody treatment led to a decrease in G-MDSCs and an increase in the proportion of CD8$^+$ T cells (figure 7C–E and online supplemental figure S7A,B). Additionally, anti-Fgl2 treatment increased the percentage of macrophages and DCs in tumors (figure 7F and G). MDSCs from anti-Fgl2 treated MC38 tumors exhibited a reduction in cholesterol content compared with control tumors (figure 7H). The 4T1 breast tumor model, known for its high infiltration of MDSCs in the TME,[29–32] was also used in our study. As expected, we observed a comparable level of tumor inhibition in the group of mice treated with anti-Fgl2 (online supplemental figure S7C). Additionally, we noticed a decrease in the infiltration of G-MDSCs in the tumors of mice treated with anti-Fgl2 antibody (online supplemental figure S7D,E). These findings indicate that Fgl2 induces ER stress and cholesterol production, potentially contributing to the expansion and activation of MDSCs.

We then explored whether blocking Fgl2 enhances the effectiveness of immune checkpoint inhibitors. The combination of anti-Fgl2 and anti-PD-1 antibodies resulted in a greater reduction in the tumor volume in mice with tumors (figure 7I). The proportion of MDSCs in the tumors was further reduced and CD8$^+$ T-cell activation was enhanced (figure 7J–M). These findings suggest that combining checkpoint blockade with Fgl2 inhibition may lead to more effective antitumor effects in vivo.

In line with these observations, TCGA analysis revealed a positive correlation between FGL2 and *CD33*, *PD-1*, *PD-L1* and *XBP1* expression (online supplemental figure S7H). Additionally, we observed increased Fgl2 expression in MDSCs from the peripheral blood of patients with CRC (online supplemental figure S7G,H). These findings suggested that Fgl2 regulates the differentiation and immunosuppressive function of MDSCs through ER stress and cholesterol production (figure 7N and online supplemental figure S7I).

DISCUSSION

MDSCs are a group of immature myeloid cells with immunosuppressive activity and play a crucial role in suppressing the antitumor immune response.[33] Depleting MDSCs through neutralizing antibodies or functional inhibition can lead to an improvement in antitumor T-cell responses.[34] In our study, we observed tumor-derived or microenvironment-derived Fgl2 promoted

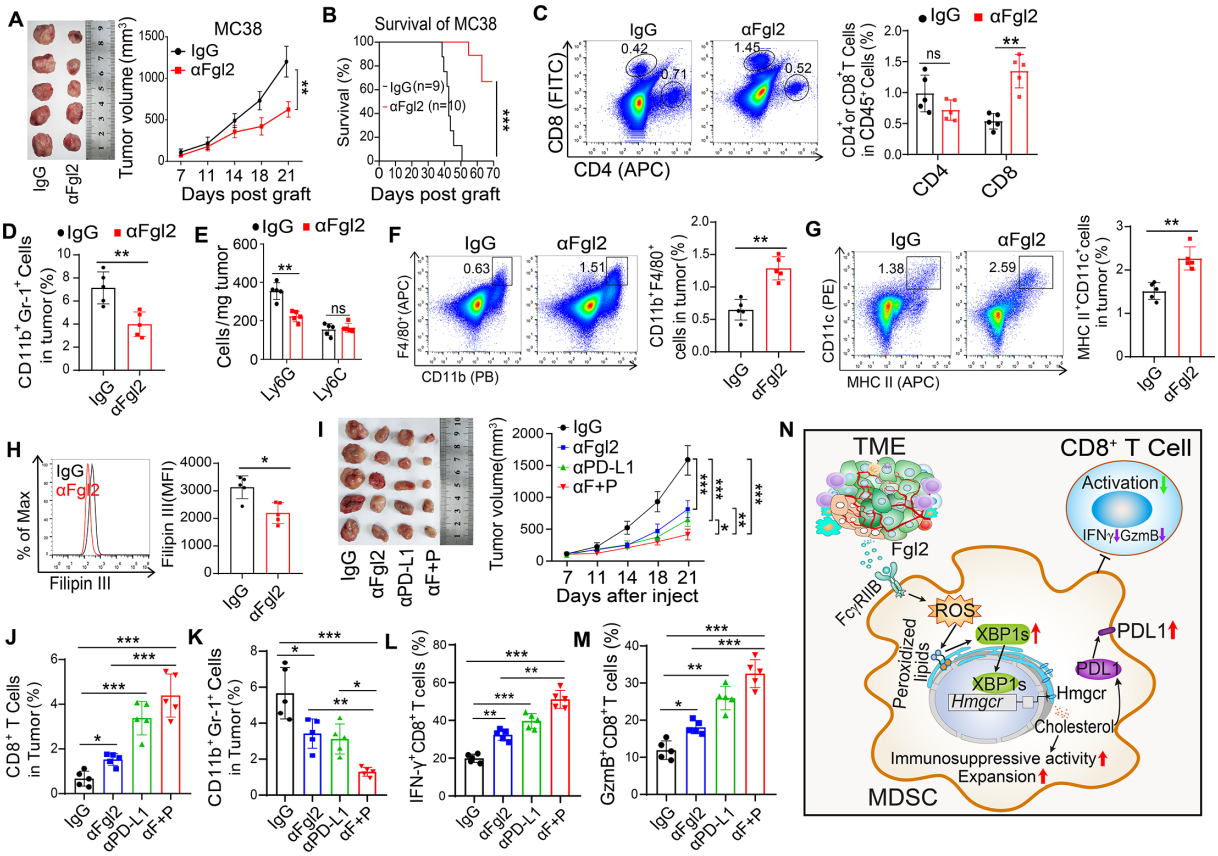

Figure 7 Inhibition of Fgl2 signaling improves the antitumor effect of immune checkpoint inhibitors. (A–H) MC38 tumor cells were injected subcutaneously into C57BL/6 mice, the mice were administered 100 µg anti-FGL2 (αFGL2) or IgG every 3 days after the tumor size reached 100 mm^3. Tumor growth (A), survival of MC38 tumor-bearing mice (B, n=9–10), percentage of CD4$^+$ and CD8$^+$ T cells (C), MDSCs (D), absolute number of G-MDSC and M-MDSC cells (E), macrophages (F) and DCs (G) in tumors, Filipin III staining of MDSCs (H), n=5. (I–M) WT mice were subcutaneously injected with MC38 tumor cells. Tumor-bearing mice were injected with IgG, anti-Fgl2 (αFgl2), anti-PD-L1 (αPD-L1), or a combination of αFGL2 and anti-PD-L1 (αF+P). Tumor growth was monitored (I), and the percentages of CD8$^+$ T cells (J), MDSCs (K), CD8$^+$ T cells producing IFN-γ (L) and GzmB (M) in the tumor tissues were analyzed by FCM (n=5). (N) Fgl2 promotes the generation and immune suppressive effects of MDSCs via cholesterol metabolism and XBP1 signaling. Data are expressed as mean±SD. *p<0.05; **p<0.01; ***p<0.001; ns, no significant difference, by two-tailed unpaired Student's t-test (A, C–H), log-rank (Mantel-Cox) test (B), one-way or two-way analysis of variance with Sidak multiple comparisons test was used to evaluate statistical significance (I–M). FCM, flow cytometry; Fgl2, fibrinogen-like protein 2; G-MDSCs, granulocytic myeloid-derived suppressor cell; KO, knockout; MDSCs, myeloid-derived suppressor cells; M-MDSC, monocytic myeloid-derived suppressor cell; WT, wild-type.

tumor progression in a CD8$^+$ T cell-dependent manner. Fgl2 deficiency reduced MDSC accumulation and increased CD8$^+$ T cell percentages in tumors. The lack of Fgl2 in the TME inhibits MDSC immunosuppressive activity and promotes MDSC differentiation into mature macrophages and DCs. Fgl2 promotes the generation of ROS and lipid peroxidation, thereby activating the XBP1 signaling pathway in MDSCs. The activation of XBP1 signaling increases the expression of genes related to cholesterol metabolism, resulting in the expansion and immunosuppressive properties of MDSCs. Blocking Fgl2 signaling results in decreased cholesterol production, leading to reduced expansion and activation of MDSCs. These findings suggested that Fgl2 plays a crucial role in determining the differentiation and immunosuppressive functions of MDSCs.

The TME is a unique environment characterized by a lack of nutrients, low oxygen levels, high acidity, and weakened immune system.[35] To survive and grow within this environment, tumor cells have adapted by reprogramming their metabolism to support their proliferation and differentiation despite the lack of nutrients and hypoxic conditions.[17] To compete for the nutrients and oxygen in the TME, immune cells force to adapt their metabolism. Metabolic reprogramming is essential for the maintenance of immunosuppressive and protumorigenic functions of MDSCs in the TME.[4] A recent study has revealed that MDSCs upregulate FAO as their primary energy source to support their immunosuppressive activities.[36] Inhibition of FAO causes a delay in MDSC suppression and tumor growth.[4] Our present data suggested that MDSCs deficient in Fgl2 showed increased FAO, but decreased expression of FAS and genes related to cholesterol biosynthesis. Interestingly, our study indicated that MDSCs had higher levels of cholesterol than HPCs, administration of cholesterol promoted

the accumulation and immunosuppressive functions of G-MDSCs. Previous studies have reported that treatment with cholesterol significantly increased the percentage of MDSCs, upregulated the phosphorylation level of STAT3, and enhanced intracellular ROS in MDSCs.[37–39] In line with these findings, our study demonstrated that MDSCs treated with cholesterol exhibited heightened immunosuppressive properties, and cholesterol also facilitated the expansion of G-MDSCs. These results suggested that Fgl2 reprograms cholesterol metabolism to support the accumulation and immunosuppressive functions of MDSCs in the TME.

Activation of ER stress has been identified as a prevalent feature of tumor-infiltrating MDSCs in vivo.[40] This stress response helps MDSCs survive in the harsh TME, characterized by nutrient deprivation, hypoxia, and acidosis.[4] Notably, MDSCs also exploit the ER stress response to acquire an immunosuppressive phenotype.[41] For example, in tumor-bearing mice, thapsigargin, an ER stressor, enhances the accumulation and immunosuppressive activity of MDSCs.[40] The IRE1α-XBP1 pathway is the most evolutionarily conserved branch of ER stress.[42] Previous studies have shown that activation XBP1 signaling promotes the expression of multiple genes that control lipid metabolism, including FASN, HMGCR, and HMGCS.[37 43] In addition, increased XBP1 levels in DCs can lead to abnormal lipid accumulation and decreased immunostimulatory activity, which in turn promotes ovarian cancer progression.[28] Our study revealed that Fgl2 induces XBP1 activation and cholesterol biosynthesis in MDSCs through ROS-mediated lipid peroxidation. Targeting XBP1 signaling in MDSCs promotes their differentiation into macrophages and DCs and reduces their immunosuppressive activity, thereby delaying tumor growth.[44]

Literature have provided evidence that Fgl2 enhances the production of mitochondrial ROS in macrophages.[44 45] ROS is primarily generated by the NADPH oxidase NOX-2 in MDSCs.[46] Consistent with these findings, our study revealed that MDSCs lacking Fgl2 exhibited lower levels of intracellular ROS and NOX-2 expression within the TME. Interestingly, we also observed a significant increase in the transcripts of antioxidant enzymes GPX4, catalase, and Sod1 in Fgl2-deficient MDSCs. Another recently published article demonstrated that Fgl2 may selectively localize to mitochondria, where it interacts with mitochondrial HSP90, thereby impeding the interaction between HSP90 and its target protein Akt.[45] Consequently, Fgl2 inhibits Akt phosphorylation and induces mitochondrial dysfunction in macrophages. Considering that FcγRIIB serves as a receptor for Fgl2, it is plausible to speculate that Fgl2 may bind to the surface of MDSCs through FcγRIIB. Subsequently, Fgl2 is endocytosed into the cell and localizes to the mitochondria, leading to alterations in mitochondrial membrane permeability and ROS generation.[47] Therefore, our results shed light on the role of Fgl2 in promoting mitochondrial dysfunction and ROS production in MDSCs.

In summary, the present study revealed that Fgl2 plays a significant role in the activation and differentiation of MDSCs by activating XBP1 signaling and cholesterol metabolism. Fgl2 acts as a mediator of XBP1 signaling and cholesterol metabolism in the TME, promoting ROS-mediated lipid peroxidation and the activation of XBP1 signaling in MDSCs. By targeting Fgl2 or cholesterol synthesis, the accumulation and immunosuppressive activity of MDSCs can be inhibited. These results suggest that Fgl2 could be a potential therapeutic target for immunotherapy, and inhibiting Fgl2 could enhance the antitumor response of the anti-PD-1 antibody.

Acknowledgements The authors appreciate Jiongming Chen and Yijiao Chen for their assistance in animal experiments.

Contributors Y.L. and L.W. conceived of the study and wrote the manuscript. J.L., L.W., N.Z., X.L., and J.Z. performed cells and animal experiments; H.Z., N.Z., X.L., and H.D. performed WB and RT-qPCR experiments; N.Z. and X.L. performed bioinformatics analysis; L.W. and J.Z. performed flow cytometry experiments. Y.L. and L.W. analyzed the data. All authors reviewed and edited the manuscript. Y.L. and L.W. are responsible for the overall content as the guarantors with full responsibility for the work and/or the conduct of the study, capability of accessing the data, and controlling the decision to publish.

Funding This work was supported by the Major International (Regional) Joint Research Program of the National Natural Science Foundation of China (No. 81920108027), National Natural Science Foundation of China (No. 82271885), Chongqing Outstanding Youth Foundation (No. cstc2020jcyj-jqX0030), Natural Science Foundation of Chongqing (No. cstc2021jcyj-msxmX0111), and Funding for Chongqing Youth Talents (No. CQYC202003006).

Competing interests None declared.

Patient consent for publication Not applicable.

Ethics approval Peripheral blood samples were collected from healthy adult volunteers and patients with colorectal cancer (CRC) at Chongqing University Cancer Hospital in China. The experiments were conducted in compliance with local, national, and international regulations, and were approved by the Ethics Committee of the hospital under protocol CZLS2022114-A. All patients provided written informed consent in accordance with the Declaration of Helsinki before enrollment in the study. Participants gave informed consent to participate in the study before taking part.

Provenance and peer review Not commissioned; externally peer reviewed.

Data availability statement Data are available upon reasonable request.

ORCID iDs
Lei Wu http://orcid.org/0000-0002-0818-7338
Yongsheng Li http://orcid.org/0000-0003-2175-9449

REFERENCES

1 García-Ortiz A, Rodríguez-García Y, Encinas J, *et al*. The role of tumor Microenvironment in multiple myeloma development and progression. *Cancers (Basel)* 2021;13:217.
2 Gabrilovich DI, Nagaraj S. Myeloid-derived Suppressor cells as regulators of the immune system. *Nat Rev Immunol* 2009;9:162–74.
3 Kramer ED, Abrams SI. Granulocytic myeloid-derived Suppressor cells as negative regulators of anticancer immunity. *Front Immunol* 2020;11:1963.
4 Veglia F, Sanseviero E, Gabrilovich DI. Myeloid-derived Suppressor cells in the era of increasing myeloid cell diversity. *Nat Rev Immunol* 2021;21:485–98.
5 Liu C-Y, Wang Y-M, Wang C-L, *et al*. Population alterations of L-Arginase- and inducible nitric oxide synthase-expressed Cd11B+/Cd14⁻/Cd15+/Cd33+ myeloid-derived Suppressor cells and Cd8+ T lymphocytes in patients with advanced-stage non-small cell lung cancer–Population alterations of L-Arginase- and inducible nitric oxide synthase-expressed Cd11B+/Cd14⁻/Cd15+/Cd33+ myeloid-derived Suppressor cells and Cd8+ T lymphocytes in patients with advanced-stage non-small cell lung cancer . *J Cancer Res Clin Oncol* 2010;136:35–45.
6 Diaz-Montero CM, Salem ML, Nishimura MI, *et al*. Increased circulating myeloid-derived Suppressor cells correlate with clinical cancer stage, metastatic tumor burden, and doxorubicin-cyclophosphamide chemotherapy. *Cancer Immunol Immunother* 2009;58:49–59.
7 Condamine T, Gabrilovich DI. Molecular mechanisms regulating myeloid-derived Suppressor cell differentiation and function. *Trends Immunol* 2011;32:19–25.
8 Yan G, Zhao H, Zhang Q, *et al*. A Ripk3-PGE(2) circuit mediates myeloid-derived Suppressor cell-potentiated colorectal carcinogenesis. *Cancer Res* 2018;78:5586–99.
9 Gabrilovich DI. Myeloid-derived Suppressor cells. *Cancer Immunol Res* 2017;5:3–8.
10 Turbitt WJ, Collins SD, Meng H, *et al*. Increased Adiposity enhances the accumulation of Mdscs in the tumor Microenvironment and Adipose tissue of Pancreatic tumor-bearing mice and in immune organs of tumor-free hosts. *Nutrients* 2019;11:3012.
11 Yan J, Zhao Q, Wang J, *et al*. Fgl2-wired Macrophages Secrete Cxcl7 to regulate the stem-like Functionality of glioma cells. *Cancer Lett* 2021;506:83–94.
12 Farley CR, Morris AB, Tariq M, *et al*. FcγRIIB is a T cell Checkpoint in antitumor immunity. *JCI Insight* 2021;6:e135623.
13 Morris AB, Farley CR, Pinelli DF, *et al*. Signaling through the inhibitory FC receptor FcγRIIB induces $Cd8^+$ T cell apoptosis to limit T cell immunity. *Immunity* 2020;52:136–50.
14 Wang M, Liu J, Xi D, *et al*. Adenovirus-mediated artificial microRNA against human fibrinogen like protein 2 inhibits hepatocellular carcinoma growth. *J Gene Med* 2016;18:102–11.
15 Yan J, Kong L-Y, Hu J, *et al*. Fgl2 as a Multimodality regulator of tumor-mediated immune suppression and therapeutic target in gliomas. *J Natl Cancer Inst* 2015;107:djv137.
16 Yan G, Zhao H, Zhang Q, *et al*. A Ripk3-Pge2 circuit mediates myeloid-derived Suppressor cell-potentiated colorectal carcinogenesis. *Cancer Res* 2018;78:5586–99.
17 Wu L, Zhang X, Zheng L, *et al*. Ripk3 Orchestrates fatty acid metabolism in tumor-associated Macrophages and Hepatocarcinogenesis. *Cancer Immunol Res* 2020;8:710–21.
18 Bruning U, Morales-Rodriguez F, Kalucka J, *et al*. Impairment of angiogenesis by fatty acid synthase inhibition involves mTOR Malonylation. *Cell Metab* 2018;28:866–80.
19 Zhu Y, Zhou J, Feng Y, *et al*. Control of intestinal inflammation, colitis-associated tumorigenesis, and macrophage polarization by fibrinogen-like protein 2. *Front Immunol* 2018;9:87.
20 Khaled YS, Ammori BJ, Elkord E. Myeloid-derived Suppressor cells in cancer: recent progress and prospects. *Immunol Cell Biol* 2013;91:493–502.
21 Zhou Z, French DL, Ma G, *et al*. Development and function of myeloid-derived Suppressor cells generated from Mouse embryonic and hematopoietic stem cells. *Stem Cells* 2010;28:620–32.
22 Li K, Shi H, Zhang B, *et al*. Myeloid-derived Suppressor cells as immunosuppressive regulators and therapeutic targets in cancer. *Signal Transduct Target Ther* 2021;6:362.
23 Condamine T, Mastio J, Gabrilovich DI. Transcriptional regulation of myeloid-derived Suppressor cells. *J Leukoc Biol* 2015;98:913–22.
24 Netea-Maier RT, Smit JWA, Netea MG. Metabolic changes in tumor cells and tumor-associated Macrophages: A mutual relationship. *Cancer Lett* 2018;413:102–9.
25 Bader JE, Voss K, Rathmell JC. Targeting metabolism to improve the tumor Microenvironment for cancer Immunotherapy. *Mol Cell* 2020;78:1019–33.
26 Mohamed E, Sierra RA, Trillo-Tinoco J, *et al*. The unfolded protein response mediator PERK governs myeloid cell-driven immunosuppression in tumors through inhibition of STING signaling. *Immunity* 2020;52:668–82.
27 Ramakrishnan R, Tyurin VA, Veglia F, *et al*. Oxidized lipids block antigen cross-presentation by Dendritic cells in cancer. *J Immunol* 2014;192:2920–31.
28 Cubillos-Ruiz JR, Silberman PC, Rutkowski MR, *et al*. ER stress sensor Xbp1 controls anti-tumor immunity by disrupting Dendritic cell homeostasis. *Cell* 2015;161:1527–38.
29 Zhang R, Dong M, Tu J, *et al*. PMN-Mdscs modulated by Ccl20 from cancer cells promoted breast cancer cell Stemness through Cxcl2-Cxcr2 pathway. *Signal Transduct Target Ther* 2023;8:97.
30 Hsu Y-L, Yen M-C, Chang W-A, *et al*. Cxcl17-derived Cd11B(+)Gr-1(+) myeloid-derived Suppressor cells contribute to lung metastasis of breast cancer through platelet-derived growth factor-BB. *Breast Cancer Res* 2019;21:23.
31 Khaki Bakhtiarvand V, Ramezani-Ali Akbari K, Amir Jalali S, *et al*. Myeloid-derived Suppressor cells (Mdscs) depletion by Cabozantinib improves the efficacy of anti-Her2 antibody-based Immunotherapy in a 4T1-Her2 murine breast cancer model. *Int Immunopharmacol* 2022;113(Pt B):109470.
32 Wu Y, Zhang C, Liu X, *et al*. Arih1 signaling promotes anti-tumor immunity by targeting PD-L1 for Proteasomal degradation. *Nat Commun* 2021;12:2346.
33 Noy R, Pollard JW. Tumor-associated Macrophages: from mechanisms to therapy. *Immunity* 2014;41:49–61.
34 Lu T, Ramakrishnan R, Altiok S, *et al*. Tumor-infiltrating myeloid cells induce tumor cell resistance to cytotoxic T cells in mice. *J Clin Invest* 2011;121:4015–29.
35 Schulz M, Salamero-Boix A, Niesel K, *et al*. Microenvironmental regulation of tumor progression and therapeutic response in brain metastasis. *Front Immunol* 2019;10:1713.
36 Al-Khami AA, Zheng L, Del Valle L, *et al*. Exogenous lipid uptake induces metabolic and functional Reprogramming of tumor-associated myeloid-derived Suppressor cells. *Oncoimmunology* 2017;6:e1344804.
37 Yang Z, Huo Y, Zhou S, *et al*. Cancer cell-intrinsic Xbp1 drives immunosuppressive Reprogramming of Intratumoral myeloid cells by promoting cholesterol production. *Cell Metab* 2022;34:2018–35.
38 Mok EHK, Leung CON, Zhou L, *et al*. Caspase-3-induced activation of Srebp2 drives drug resistance via promotion of cholesterol biosynthesis in hepatocellular carcinoma. *Cancer Res* 2022;82:3102–15.
39 Nakayama H, Sekine Y, Oka D, *et al*. Combination therapy with novel androgen receptor antagonists and Statin for Castration-resistant prostate cancer. *Prostate* 2022;82:314–22.
40 Chen X, Cubillos-Ruiz JR. Endoplasmic Reticulum stress signals in the tumour and its Microenvironment. *Nat Rev Cancer* 2021;21:71–88.
41 Bettigole SE, Glimcher LH. Endoplasmic Reticulum stress in immunity. *Annu Rev Immunol* 2015;33:107–38.
42 Chopra S, Giovanelli P, Alvarado-Vazquez PA, *et al*. Ire1Alpha-Xbp1 signaling in leukocytes controls prostaglandin biosynthesis and pain. *Science* 2019;365:eaau6499.
43 Lee AH, Iwakoshi NN, Glimcher LH. XBP-1 regulates a subset of Endoplasmic Reticulum resident chaperone genes in the unfolded protein response. *Mol Cell Biol* 2003;23:7448–59.
44 Hu J, Wang H, Li X, *et al*. Fibrinogen-like protein 2 aggravates Nonalcoholic Steatohepatitis via interaction with Tlr4, eliciting inflammation in Macrophages and inducing hepatic lipid metabolism disorder. *Theranostics* 2020;10:9702–20.
45 Tao R, Han M, Yuan W, *et al*. Fibrinogen-like protein 2 promotes proinflammatory macrophage polarization and mitochondrial dysfunction in liver fibrosis. *Int Immunopharmacol* 2023;117:109631.
46 Ugolini A, Tyurin VA, Tyurina YY, *et al*. Polymorphonuclear myeloid-derived Suppressor cells limit antigen cross-presentation by Dendritic cells in cancer. *JCI Insight* 2020;5:e138581.
47 Chang C-P, Yang M-C, Liu H-S, *et al*. Concanavalin A induces Autophagy in hepatoma cells and has a therapeutic effect in a murine in situ hepatoma model. *Hepatology* 2007;45:286–96.